Synthesis and ex vivo biodistribution of two 68Ga-labeled tetrazine tracers : comparison of pharmacokinetics

Lambidis, Elisavet

2022-12

Lambidis , E , Lumen , D , Koskipahta , E , Imlimthan , S , B. Lopez , B , Fraguas-Sanchez , A I , Sarparanta , M , Cheng , R H & Airaksinen , A J 2022 , ' Synthesis and ex vivo biodistribution of two 68Ga-labeled tetrazine tracers : comparison of pharmacokinetics ' , Nuclear Medicine and Biology , vol. 114 , pp. 151-161 . https://doi.org/10.1016/j.nucmedbio.2022.05.004

http://hdl.handle.net/10138/356061
https://doi.org/10.1016/j.nucmedbio.2022.05.004

Nuclear Medicine and Biology 114-115 (2022) 151–161

Contents lists available at ScienceDirect

Nuclear Medicine and Biology

journal homepage: www.elsevier.com/locate/nucmedbio

Synthesis and *ex vivo* biodistribution of two ^{68}Ga-labeled tetrazine tracers: Comparison of pharmacokinetics

Elisavet Lambidis [a], Dave Lumén [a], Elina Koskipahta [a], Surachet Imlimthan [a], Brianda B. Lopez [a], Ana Isabel Fraguas Sánchez [a], Mirkka Sarparanta [a], R. Holland Cheng [b], Anu J. Airaksinen [a,c,*]

[a] Department of Chemistry, Radiochemistry, University of Helsinki, Helsinki FI-00014, Finland
[b] Department of Molecular and Cellular Biology, University of California, Davis, CA 95616, USA
[c] Turku PET Centre, Department of Chemistry, University of Turku, Turku FI-20520, Finland

ARTICLE INFO

Keywords:
PET imaging
Gallium-68
HBED-CC
DOTA
Tetrazine
IEDDA ligation
nanoparticles

ABSTRACT

Pretargeted PET imaging allows the use of radiotracers labeled with short-living PET radionuclides for tracing drugs with slow pharmacokinetics. Recently, especially methods based on bioorthogonal chemistry have been under intensive investigation for pretargeted PET imaging. The pharmacokinetics of the radiotracer is one of the factors that determine the success of the pretargeted strategy. Here, we report synthesis and biological evaluation of two ^{68}Ga-labeled tetrazine (Tz)-based radiotracers, [^{68}Ga]Ga-HBED-CC-PEG$_4$-Tz ([^{68}Ga]**4**) and [^{68}Ga]Ga-DOTA-PEG$_4$-Tz ([^{68}Ga]**6**), aiming for development of new tracer candidates for pretargeted PET imaging based on the inverse electron demand Diels-Alder (IEDDA) ligation between a tetrazine and a strained alkene, such as *trans*-cyclooctene (TCO). Excellent radiochemical yield (RCY) was obtained for [^{68}Ga]**4** (RCY > 96%) and slightly lower for [^{68}Ga]**6** (RCY > 88%). Radiolabeling of HBED-CC-Tz proved to be faster and more efficient under milder conditions compared to the DOTA analogue. The two tracers exhibited excellent radiolabel stability both *in vitro* and *in vivo*. Moreover, [^{68}Ga]**4** was successfully used for radiolabeling two different TCO-functionalized nanoparticles *in vitro*: Hepatitis E virus nanoparticles (HEVNPs) and porous silicon nanoparticles (PSiNPs).

1. Introduction

Positron emission tomography (PET) has multiple benefits in diagnostic applications. PET has an outstanding sensitivity compared to most of the bioimaging techniques—such as single-photon emission computed tomography (SPECT), fluorescence, ultrasound, and magnetic resonance—and it is a functional imaging modality allowing quantitative evaluation of imaging agent distribution *in vivo* [1,2]. Most of the radionuclides utilized in PET imaging have short physical half-lives, which limit their uses for the *in vivo* investigation of relatively quick biological processes. For example, the PET evaluation of new drug candidates with slow pharmacokinetics like antibodies requires the use of long-living positron emitters, which can cause unnecessary radiation exposure to the subject under study. As a solution, pretargeted PET imaging has been investigated. In pretargeted imaging, radiolabeling of a targeting vector or drug candidate is done *in vivo* by harnessing specific reactions between the targeting vector and the radiotracer. Bioorthogonal chemistry-based strategies have proved their applicability, and several successful examples on pretargeted PET imaging using antibodies, nanoparticles, and other targeting vectors have already been reported. Most have utilized the inverse electron-demand Diels-Alder (IEDDA) ligation between a tetrazine (Tz) and a strained alkene, such as *trans*-cyclooctene (TCO) [3–13]. The reaction between Tz and TCO takes place rapidly, and the formed cycloaddition product is highly stable. Typically, the TCO is conjugated to a targeting vector while the Tz carries the radiolabel. Determined by the pharmacokinetics of the targeting vector, sufficient time is required after the vector administration to ensure that it has adequately accumulated to the target site and cleared from the circulation. Clearance from circulation is important in order to avoid radiolabeling of the vector in the blood, resulting in increased background radioactivity levels in non-target regions. After completed target accumulation, a second injection containing the small molecule Tz radiotracer is given, optimally followed by rapid covalent ligation with the vector and clearance of the unbound tracer from the body [11–14]. This approach offers high specificity in terms of targeting while minimizing the residence time of the radiotracer in the

* Corresponding author at: Turku PET Centre, Department of Chemistry, University of Turku, Turku FI-20520, Finland.
E-mail address: anu.airaksinen@utu.fi (A.J. Airaksinen).

https://doi.org/10.1016/j.nucmedbio.2022.05.004
Received 28 November 2021; Received in revised form 18 May 2022; Accepted 19 May 2022
Available online 24 May 2022

surrounding healthy tissues, hence reducing the radiation burden. Nevertheless, there are several factors that affect the success of the pretargeted imaging strategy, one of which is the pharmacokinetics of the radiotracer that can influence the IEDDA reaction efficiency *in vivo* as well as the non-specific background activity caused by the unreacted radiotracer and its radio-metabolites [11,12].

Gallium-68 (^{68}Ga) is a small (ionic radius: 0.62 Å) and short-lived (half-life 67.8 min) radionuclide. ^{68}Ga has high positron energy (E_{max} = 1.90 MeV) and positron yield of 89%. It is a hard Lewis acid, and thus it has a coordination preference toward carboxylates, phosphonates, and other hard Lewis bases, resulting in highly stable complex structures [15–18]. The stability of ^{68}Ga complexes is crucial because $^{68}Ga^{3+}$ has a similar ionic radius to trivalent iron (Fe^{3+}, 0.65 Å) [15]. Free $^{68}Ga^{3+}$ in the blood mimics the ferric cation and binds to transferrin. Due to the incapability of $^{68}Ga^{3+}$ to be reduced *in vivo*, it remains bound to the iron-transport protein, and thus, it gets transported throughout the body [19,20].

Typical chelators for $^{68}Ga^{3+}$ are DOTA (1,4,7,10-tetraazacyclododecane-1,4,7,10-tetraacetic acid), NOTA (1,4,7-triazacyclononane-1,4,7-triacetic acid), DTPA (diethylenetriamine pentaacetate) and DFO (desferrioxamine), although the last two chelators have shown suboptimal *in vivo* stability and slow blood clearance [1,2,15,17,21]. In pretargeted PET imaging various chelator-conjugated tetrazines have been used. For instance, tetrazines have been involved in the radiolabeling of TCO-bearing antibodies and peptides, such as in the case of the ^{68}Ga-NOTA-PEG$_{11}$-Tz [22], DOTA-GA (GA: glutaric acid) and ^{68}Ga-NODA-GA tracers [23]. Additionally, it has been shown that multimeric tetrazine conjugates can improve the radiolabeling efficiency of peptides [6].

DOTA is a cyclen-based chelator and the most extensively used chelating agent for PET imaging with ^{68}Ga. In theory, the cavity of DOTA is relatively large to host a small radiometal like gallium. However, the coordination bonds between the donor atoms (N and O) and ^{68}Ga are strong enough for the formed complex to be sufficiently stable *in vivo*. Although the ^{68}Ga-labeling of a DOTA complex can be very efficient [24], no product is obtained at ambient temperature, and typically the radiolabeling requires high temperatures and low pH for a complete reaction to take place. The harsh conditions can cause complications in biomolecule radiolabeling where disintegration or compromise of targeting ability can occur, while radiolabeling at low temperature decreases the radiochemical conversion and yield [2,3,7].

More recently, the HBED (*N*,*N*′-bis(2-hydroxybenzyl)ethylendiamin-N,N′-diacetic acid) chelator was introduced for radiolabeling with ^{68}Ga [15,17]. HBED molecule is based on the EDTA (ethylenediaminetetraacetic acid, 2-[2-[bis(carboxymethyl)amino]ethyl-(carboxymethyl) amino]acetic acid) structure with two phenolic groups substituting two of the carboxylic acids. The substitution increases the stability of HBED-radiometal complexes, like in the case of [^{68}Ga]Ga-HBED [15]. Another benefit is the capability of acyclic HBED to give rise to exceptionally fast and quantitative radiolabeling reactions just at room temperature [25]. In addition, the observed high *in vitro* and *in vivo* stability has prompted further optimization of the chelator structure. Closely related to HBED, HBED-CC (*N*,*N*′-bis-[2-hydroxy-5-(carboxyethyl) benzyl]ethylenediamine-N,N′-diacetic acid) chelator, which contains two additional propionic acid groups, comprises all the HBED benefits while it can act as a bifunctional chelator for ^{68}Ga [26–35]. In terms of complex formation kinetics, HBED-CC has been compared to the well-established $^{68}Ga^{3+}$ chelator, NOTA. These two ^{68}Ga-labeled complexes have shown highly comparable properties in terms of *in vitro* stability, cell uptake, and biodistribution with a lower liver uptake of [^{68}Ga]Ga-HBED-CC tracers [15,17,25,36–38].

In this study, the aim was the development of two different ^{68}Ga-labeled Tz-based radiotracers bearing the HBED-CC and DOTA chelators (Fig. 1), and the comparison of their pharmacokinetics in mouse models as a prerequisite for their future use in pretargeted PET imaging applications. Additionally, as further evidence for their potential use in bioorthogonal chemistry, two TCO-bearing nanoparticles (NPs) were radiolabeled using both radiotracers. The NPs in this case were the Hepatitis E virus nanoparticles (HEVNPs) and porous silicon nanoparticles (PSiNPs). Overall, the HBED-CC-based radiotracer was shown to be superior to the DOTA-based radiotracer in terms of radiolabeling efficiency and molar activity, improving the sensitivity of the tracer to detect a targeting vector even at low TCO concentrations.

2. Materials and methods

All chemicals and solvents were obtained from commercial providers and used without further purification. Tz-PEG$_4$-NH$_2$ (N-(4-(1,2,4,5-tetrazin-3-yl)benzyl)-1-amino-3,6,9,12-tetraoxapentadecan-15-amide) was from Conju-Probe, LLC (San Diego, CA, U.S.A.). HBED-CC-tris(*tBu*) ester (3-(3-{[(2-{[5-(2-tert-Butoxycarbonyl-ethyl)-2-hydroxy-benzyl]-tert-butoxy-carbonylmethyl-amino}-ethyl)-*tert*-butoxycarbonylmethyl-amino]-methyl}-4-hydroxy-phenyl)-propionic acid) was purchased from ABX (Radeberg, Germany). DOTA-NHS ester (1,4,7,10-tetraazacyclododecane-1,4,7,10-tetraacetic acid mono-N-hydroxysuccinimide ester) was purchased from Macrocyclics (Plano, TX, U.S.A.), and TCO-PEG$_4$-NHS ester from Jena Bioscience (Jena, Germany). Other chemicals were purchased mainly from Sigma-Aldrich (St. Louis, MO, U.S.A.). All the water used was ultra-pure (>18.2 MΩ cm^{-1}) and was prepared on a Milli-Q (MQ) Integral 10 water purification system. For each buffer preparation, MQ water was treated with Chelex® 100 sodium form

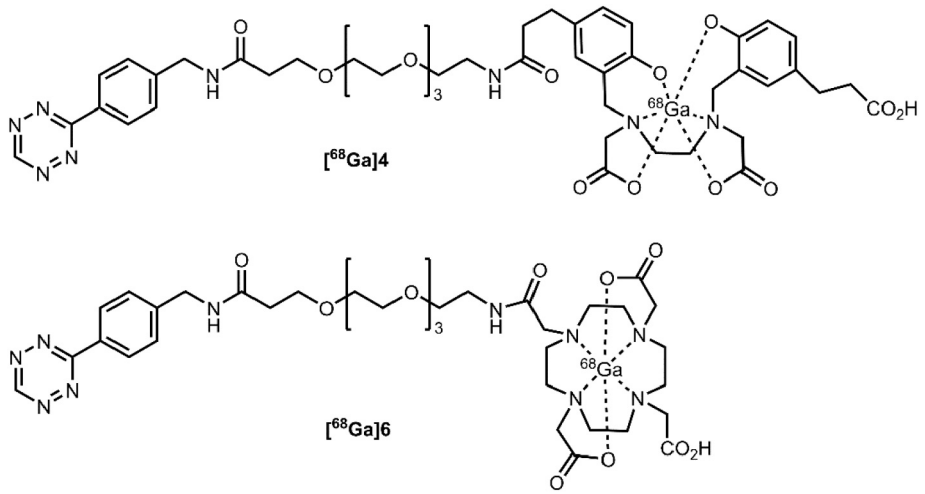

Fig. 1. The structures of [^{68}Ga]**4** and [^{68}Ga]**6** that were synthesized in this study.

(Sigma-Aldrich) at a concentration of 5 g/l for the elimination of trace metals. The Sep-Pak light C18 cartridges were from Waters Corporation (Milford, MA, U.S.A.) and preconditioned prior use with 2 ml EtOH and 5 ml MQ. The PD-10 Sephadex G-25 M desalting columns were obtained from GE Healthcare (Chicago, IL, U.S.A.) and preconditioned prior use with 20 ml MQ and 20 ml 0.01 M PBS (pH 7.4). HPLC (Shimadzu Corporation, Kyoto, Japan) was performed using a column an Altima C18 column (5 μm, 250 × 10 mm). NMR spectroscopy was done on a Varian Mercury 300 MHz or 75 MHz spectrometer from Palo Alto (CA, U.S.A.) and the spectra are shown in the supplementary material (Section 2.1, Figs. S1-S4). A Daltonics micrOTOF spectrometer from Bruker Corporation (Bremen, Germany) was used for Electrospray Ionization Time-of-Flight (ESI-ToF) MS measurements. The MS measurements were done under negative ionization mode and with sodium formate as the calibration standard. The tip sonicator was from QSonica (Newtown, CT, U.S.A.). For the transmission electron microscopy (TEM) measurements, a JEOL1400 was used from JEOL Ltd. (Akishima, Tokyo, Japan). The protein concentration was measured using a μDrop Plate on a Multiskan Sky Microplate Spectrophotometer from Thermo Scientific (Waltham, MA, USA). For the gallium elution, the water Tracer SELECT™ was acquired from Honeywell-Riedel-de Häen™ (Seelze, Germany), and the ultrapure 30% HCl (hydrochloric acid) was purchased from Merck (Kenilworth, NJ, U.S.A.). A photostimulated luminescence scanner Fuji FLA 5100 (Tokyo, Japan), was used for the digital autoradiography using a Fuji TR323309 imaging plate. The $^{68}Ge/^{68}Ga$ generators (1850 MBq at calibration) were GalliaPharm type generators produced by Eckert & Ziegler (Berlin, Germany). For the semi-automated radiosynthesis, a Modular-Lab system from Eckert & Ziegler was utilized. The automatic gamma counter was 1480 Wallac Wizard® 3″ (PerkinElmer™ Life Sciences, Waltham, MA, U.S.A.), and the measurement lasted for 60 s per tissue sample. The radiochemical conversion (RCC) was determined by radio-TLC (for both the Tz tracers and radiolabeled NPs) and radio-HPLC (for the Tz tracers) analysis of the crude product in the end of each synthesis. For the Tz tracers, the radiochemical yield (RCY) and purity (RCP) of each isolated product was analyzed by radio-TLC and radio-HPLC after the purification of the crude product. The minimum molar activity (A_m) of the Tz tracers was determined from calculations with respect to the radioactivity of the product and the amount of the precursor since no precursor separation was made from the radiolabeled product.

2.1. Hepatitis E viral nanoparticles (HEVNPs)

HEVNPs were produced as previously reported with 60 lysine amino acid residues on their surface. The size of HEVNP was approximately 27 nm in diameter [39].

2.2. Thermally hydrocarbonized porous silicon nanoparticles (UnTHCPSi NPs)

UnTHCPSi NPs were kindly prepared and provided by Prof. Jarno Salonen and Ermei Mäkilä (University of Turku, Finland). The NPs (approximately 200 nm) were produced using the pulsed electrochemical etching method as previously described [40]. Hereinafter, the UnTHCPSi particles will be abbreviated as PSiNPs.

2.3. Synthesis of Tz-PEG$_4$-HBED-CC(tBu) (3)

HBED-CC-tris(*tBu*)ester (**1**) (19.0 mg, 27 μmol, 1.5 eq.) and HATU (1-[Bis(dimethylamino)methylene]-1H-1,2,3-triazolo[4,5-*b*]pyridinium 3-oxid hexafluoro-phosphate) (12.3 mg, 32 μmol, 1.8 eq.) were weighted into an oven-dried 10-ml round bottom flask. Anhydrous DMF (dimethylformamide) was added (2 ml) and the mixture was stirred for 10 min at room temperature (RT). Tz-PEG$_4$-NH$_2$ (**2**) (8.5 mg, 18 μmol, 1 eq.) dissolved in DMF (1 ml) was added dropwise. The mixture was stirred for 20 min at RT after which DIPEA (N,N-Diisopropylethylamine) was added (9.4 μl, 54 μmol, 3 eq.) and the reaction mixture was stirred in dark, at RT and under inert atmosphere for 48 h. The reaction was monitored by silica TLC (DCM:MeOH, 20:1) until **2** was consumed. EtOAc was added in the reaction flask (10 ml) and the organic layer was extracted three times with 5 ml 5% LiCl. Magnesium sulfate was added to dry the organic phase. The organic layer was filtered and purified with a silica column with DCM:MeOH (20:1) as eluent. The solvent was evaporated yielding the pink product (**3**) with 79% yield (15.9 mg, 14 μmol). ^{1}H NMR(**3**) (300 MHz, $CDCl_3$) δ 10.20 (s, 1H), 8.58, 8.56 (d, 2H), 7.54, 7.52 (d, 2H), 7.00 (br, 2H), 6.75 (br, 4H), 4.58, 4.56 (d, 2H), 3.77–3.69 (m, 8H), 3.61–3.47 (m, 12H), 3.17 (br, 6H), 2.79–2.68 (m, 8H), 2.46–2.40 (m, 6H), 1.41 (s, 27H) ppm. ^{13}C NMR(**3**) (75 MHz, $CDCl_3$) δ 172.98, 172.54, 171.97, 170.10, 157.91, 155.83, 131.67, 129.31, 128.43, 121.70, 116.50, 82.19, 70.59, 67.44, 58.17, 55.61, 50.52, 43.09, 39.49, 39.33, 38.99, 38.81, 37.59, 37.12, 30.40, 28.22 ppm.

2.4. Synthesis of Tz-PEG$_4$-HBED-CC (4)

In an oven-dried 10-ml round-bottom flask **3** (3.9 mg, 3.5 μmol) was dissolved in 3.5 ml of 20% TFA and 80% anhydrous DCM. The reaction mixture was stirred overnight in dark, at RT, and under an inert atmosphere. The reaction was monitored by silica TLC (DCM:MeOH, 1:0.1) until it was complete. Bromocresol green stain solution in ethanol was used for staining. **4** was isolated as a pink solid with 98% yield (3.2 mg, 3.4 μmol). ^{1}H NMR(**4**) (300 MHz, CD_3OD) δ 10.31 (s, 1H), 8.55, 8.52 (d, 2H), 7.58, 7.55 (d, 2H), 7.10 (br, 4H), 6.81 (br, 2H), 2.23 (br, 2H), 4.13–4.07 (m, 8H), 3.67–3.60 (m, 12H), 2.81 (br, 6H), 2.56–2.41 (m, 14H) ppm. ESI-ToF-MS(**4**): $C_{46}H_{59}N_8O_{14}^-$ calculated *m/z*: 947.4229, found *m/z*: 947.4266.

2.5. Synthesis of Tz-PEG$_4$-DOTA (6)

2 (4.0 mg, 8.5 μmol, 1 eq.) and DOTA-NHS ester (**5**) (7.0 mg, 9.2 μmol, 1.08 eq.) were added into an oven-dried 25-ml round-bottom flask. DIPEA (8.9 μl, 51.0 μmol, 6 eq.) and anhydrous DMF were then added (2.0 ml). The reaction mixture was stirred overnight (16–18 h) in dark, at RT, and under an inert atmosphere. The reaction was monitored by silica TLC (DCM:MeOH, 10:1) until **2** was consumed. Bromocresol green stain solution in ethanol was used for staining the TLC. The reaction mixture was evaporated to dryness, dissolved in 30% acetonitrile, and the final product purified with HPLC (ACN:0.1% formic acid in MQ 40:60, 2 ml/min, 15 min run, R_t(**6**) = 5.1). The solvent was evaporated under reduced pressure yielding the final product (**6**) as a pink solid (yield 81%, 5.6 mg, 6.9 μmol). ^{1}H NMR(**6**) (300 MHz, $CDCl_3$) δ 10.33 (s, 1H), 8.57, 8.54 (d, 2H), 7.58, 7.60 (d, 2H), 4.54 (br, 2H), 3.80 (t, 2H), 3.74 (br, 2H), 3.64–3.61 (m, 12H), 3.60–3.57 (m, 10H), 3.55–3.48 (m, 16H), 2.56 (t, 2H) ppm. ESI-ToF-MS(**6**): $C_{36}H_{55}N_{10}O_{12}^-$ calculated *m/z*: 819.4079, found *m/z*: 819.4045.

2.6. Radiosynthesis of [^{68}Ga]Ga-HBED-CC-PEG$_4$-Tz ([^{68}Ga]4)

4 (8 μg, 8.4 nmol) was dissolved in 0.5 ml metal-free 2.5 M sodium acetate buffer (pH 5.5) in a 15-ml conical centrifuge tube. This was followed by the addition of freshly eluted $^{68}GaCl_3$ (4.5–282 MBq in 60 μl–2 ml of 0.1 M HCl). The pH of the reaction mixture was 4.5 and the mixture was incubated on a heating block for 15 min at 25 °C with mixing at 400 rpm. The reaction initiated immediately after the addition of the radionuclide eluate. The product was purified by solid phase extraction using a pre-conditioned C18 light cartridge. After loading the reaction mixture in the cartridge, the free $^{68}GaCl_3$ was washed away with 6 ml MQ. [^{68}Ga]**4** was eluted with 0.5 ml of absolute EtOH. The radiochemical conversion and purity of [^{68}Ga]**4** were analyzed by radio-TLC (iTLC-SA, ammonium acetate:MeOH 1:1 *v*/v, pre-mixed, pH 4.86, R_f([^{68}Ga]**4**) = 0.8 and R_f(free ^{68}Ga) = 0.0) and radio-HPLC (ACN:MQ 20:80, 2 ml/min, R_t([^{68}Ga]**4**) = 5.3 min), and were 98.6 ± 0.6% (*n* =

15) and 99.3 ± 0.3% (n = 19), respectively. The decay corrected radiochemical yield of [^{68}Ga]**4** was 96.7%. As an example, for a starting activity of 114 MBq, the activity of the isolated product at the end of the purification was 88 MBq. The molar activity of [^{68}Ga]**4** was 0.5–28.6 GBq/μmol at EOS.

2.7. Radiosynthesis of ([^{68}Ga]**4**) after concentrating the [^{68}Ga]$GaCl_3$ solution using strong cation exchange (SCX) chromatography

The SCX column was first pre-conditioned with 1 ml of 5.5 M HCl followed by 5 ml of MQ water. The whole amount (10 ml) of the generator-eluted $^{68}GaCl_3$ was then loaded, and the elution was done with 500 μl of 5 M NaCl solution acidified with 5.5 M HCl (12.5 μl). This eluted portion of $^{68}GaCl_3$ was then added to the dissolved precursor **4** (8 μg). Moreover, 2.5 M sodium acetate buffers at pH 4.8 and 5.0 were tested, resulting in a comparable RCC of 96.7% and 95.7% (n = 1), respectively. The RCP in both cases was kept above 99.2% after the purification with the C18 cartridge as described above (Section 2.6).

2.8. Radiosynthesis of [^{68}Ga]Ga-DOTA-PEG$_4$-Tz ([^{68}Ga]**6**)

6 (0.2 mg, 243.6 nmol) was dissolved in 2.5 ml metal-free 0.25 M ammonium acetate buffer (pH 6.8) in a 15-ml conical centrifuge tube. This was followed by the addition of freshly eluted $^{68}GaCl_3$ in 0.1 M HCl (5.5–216 MBq in 135 μl–2 ml). The reaction mixture was incubated for 15 min at 90 °C with mixing at 400 rpm on a heating block. The reaction initiated immediately after the addition of the radionuclide eluate. The reaction mixture was cooled down to RT after which the product was purified with solid phase extraction by using a C18 light cartridge. After loading the reaction mixture in the cartridge, the resin was washed with 6 ml MQ. [^{68}Ga]**6** was eluted with 0.4 ml of absolute EtOH. The radiochemical conversion and purity of [^{68}Ga]**6** were analyzed by radio-TLC (iTLC-SA, ammonium acetate:MeOH 1:1 *v*/v, pre-mixed, pH 4.86, R_f([^{68}Ga]**6**) = 0.7 and R_f(free ^{68}Ga) = 0.0) and radio-HPLC (ACN:0.1% FA (formic acid) in MQ 40:60, 2 ml/min, R_t([^{68}Ga]**6**) = 5.0 min), and were 93.3 ± 3.2% (n = 5) and 98.2 ± 0.6% (n = 5), respectively. The decay corrected radiochemical yield of [^{68}Ga]**6** was 88.9%. As an example, for a starting activity of 126 MBq, the activity of the isolated product at the end of the purification was 86 MBq. The molar activity of [^{68}Ga]**6** was 0.02–0.73 GBq/μmol at EOS.

2.9. In vitro stability of [^{68}Ga]**4** and [^{68}Ga]**6**

The radiolabel stability of [^{68}Ga]**4** and [^{68}Ga]**6** was investigated in sodium acetate and PBS buffers, respectively, in 20% and 50% human plasma and in ferric chloride hexahydrate ($FeCl_3{\cdot}6H_2O$; 18 mM in water). All the samples (n = 3 per testing solution) were of same concentration (1.5 μM for [^{68}Ga]**4** and 28.4 μM for [^{68}Ga]**6**) and were incubated at 37 °C. The amount (%) of the intact radiolabeled Tz tracers was monitored by radio-TLC up to 5 h.

2.10. Determination of log$D_{7.4}$ of [^{68}Ga]**4** and [^{68}Ga]**6**

The distribution coefficients were measured between 1-octanol and 20 mM phosphate buffer (pH 7.4) using the shake flask method. Equal volumes (5 ml) of both solvents were measured in a centrifuge tube and 200 μl of the final product were added. The tube was then shaken vigorously for 1–2 min after which the two phases were let to separate for 10 min. The activities of the organic and aqueous phases were determined with a dose calibrator and with a gamma counter. The log$D_{7.4}$ was calculated using the formula:

$$\mathrm{Log}D_{7.4} = Log\frac{[A]_{OCT}}{[A]_{PBS}}$$

Log$D_{7.4}$ of [^{68}Ga]**4** was measured in triplicate and for [^{68}Ga]**6** as a single measurement.

2.11. Evaluation of ex vivo biodistribution of [^{68}Ga]**4** and [^{68}Ga]**6**

All animal experiments were carried out under a project license approved by the National Board of Animal Experimentation in Finland (ESAVI/12132/04.10.07/2017) and in compliance with the respective institutional, national and EU regulations and guidelines. Mice were group-housed in standard polycarbonate cages with aspen bedding, nesting material (Tapvei, Harjumaa, Estonia) and enrichment (aspen blocks and disposable cardboard hut). Pelleted food (Teklad 2019C diet, Envigo, Horst, Netherlands) and tap water were available *ad libitum*. Environmental conditions of a 12:12 light/dark cycle, temperature of 22 ± 1 °C, and relative humidity of 55 ± 15% were maintained throughout the study.

The *ex vivo* biodistribution of [^{68}Ga]**4** and [^{68}Ga]**6** was evaluated in healthy female BALB/c mice (Janvier, 7–8 weeks, 16–19 g, 5 animals/time point) at four different predetermined timepoints (15–120 min) after intravenous injection of the radiotracers (0.5–2.0 MBq of [^{68}Ga]**4** or 0.3–1.2 MBq for [^{68}Ga]**6**) formulated in 200 μl of 0.01 M PBS (pH = 7.4)–10% EtOH *via* the lateral tail vein.

Mice were euthanized at 15, 30, 60 and 120 min after the injection by CO_2 asphyxiation followed by cervical dislocation. Selected organs were harvested and weighed in 5-ml liquid scintillation tubes. The radioactivity in the samples together with five weighed standards of the injected solution was counted by gamma counter with the decay corrected to the start of the measurement. Results are expressed as %ID/g of tissue.

2.12. Separation of blood components and analysis of their interaction with [^{68}Ga]**4** and [^{68}Ga]**6**

Blood samples at 15, 30, 60 and 120 min time points were collected during the *ex vivo* study. The samples were collected in 1.5-ml Protein LoBind microtubes (Eppendorf) and 1 μl of heparin solution (0.1 ml heparin 5000 IU in 9.9 ml NaCl) was added. The samples were centrifuged at 1300*g* for 10 min to obtain the red blood cells (RBCs) pellet. Cold acetonitrile was added into the supernatant. The samples were then centrifuged at 13,000*g* for 5 min to separate the pellet containing the blood proteins from the plasma supernatant. After this treatment, the radioactivity of the three blood fractions—RBCs, proteins and plasma—was counted by the gamma counter.

2.13. Conjugation of HEVNPs with TCO-PEG$_4$-NHS ester

The TCO-PEG$_4$-NHS ester reagent (16.05 nmol–1.58 μmol, 5–21 eq. per lysine, n_{Lys} = 60 per HEVNP capsid) (supplementary material Section 1.1) was dissolved in 1 μl DMSO in 100 μl phosphate buffer (PB) (0.01 M pH 7.4) and added dropwise into the HEVNP dispersion (3.21–82.65 nmol, 21.4–165.3 μM in 111–250 μl PB). The mixture was reacted at RT for 3 h and at 4 °C for 16–17 h, and the TCO-HEVNPs were purified by size exclusion chromatography on a PD-10 desalting column using 2.8 ml of 0.01 M PBS (pH 7.4) as the eluent. After the PD-10 elution, the NP concentration was measured with a μDrop Plate Spectrophotometer and was 0.8–8.7 μM or 0.041–0.5 mg/ml in 2.8 ml depending on the initial concentration. The conservation of the NP size and morphology was confirmed by TEM.

2.14. Conjugation of PSiNPs with TCO-PEG$_3$-NH$_2$

PSiNPs (1.0 mg/ml in 96% EtOH) were centrifuged (10,000*g*, 5 min) and the EtOH was removed. The PSiNP pellet was redispersed in 0.6 ml anhydrous DMF using a tip sonicator at 20% amplitude for 10 s. HATU (2.0 mg in 50 μl anhydrous DMF) and 1 μl of DIPEA were added to the NP suspension. Lastly, TCO-PEG$_3$-NH$_2$ (8.1 μmol, 3.0 mg in 3.0 μl dry DMF) was added prior the overnight incubation at RT. For the

purification, the reaction vial was centrifuged at 12,000*g* for 5 min and washed with 1 ml of 96% EtOH. Another centrifugation step was followed and the pellet this time was washed with 1 ml of MQ. The TCO-PSiNPs were then redispersed and stored in 1 ml of 96% EtOH.

2.15. Radiolabeling of HEVNPs and PSiNPs with [^{68}Ga]**4**

[^{68}Ga]**4** (8 pmol–29.6 nmol for TCO-PSiNPs or 0.03 nmol–2.2 nmol for TCO-HEVNPs) in 0.01 M PBS (pH = 7.4) with 10% EtOH was added into the NP suspension (0.1–0.3 mg, n_{TCO} = 10–30 nmol of TCO-PSiNPs or 0.01–0.2 mg, n_{TCO} = 0.55–11 nmol of TCO-HEVNPs) in 0.01 M PB (pH 7.4). The TCO:Tz molar ratio varied and was between 1:1 and 1:0.0008. The reaction mixture was incubated at 37 °C for 10 min. The IEDDA RCC was measured by radio-TLC (iTLC-SA and 50 mmol EDTA in 0.9% NaCl for PSiNPs, R_f([^{68}Ga]**4**-TCO-PSiNPs) = 0.0 and R_f(unbound [^{68}Ga]**4**) = 0.7, or Whatman 1 paper and 0.5 mM DTPA for HEVNPs, R_f([^{68}Ga]**4**-TCO-HEVNPs) = 0.0 and R_f(unbound [^{68}Ga]**4**) = 0.8).

2.16. In vitro IEDDA reactions between TCO-PSiNPs and [^{68}Ga]**4** after treating the NPs in tumor-mimicking conditions

TCO-PSiNPs were incubated up to 24 h in either sodium acetate pH 5.3 or 10% fetal bovine serum (FBS) in sodium acetate pH 5.3. Following the incubation in the tumor-simulated fluids at the different time points, 0.1 mg of TCO-PSiNPs (n_{TCO} = 10 nmol) were reacted with [^{68}Ga]Ga-HBED-CC-PEG$_4$-Tz (0.099 nmol, 0.01 eq.). The IEDDA RCC was measured by radio-TLC as described above for [^{68}Ga]**4**-TCO-PSiNPs and was kept constant at approximately 22% (in the range of 19%–24%) in all conditions and time points.

2.17. Statistical analysis

The mean values of the quantitative data were analyzed for statistical significance using an unpaired two-tailed *t*-test on GraphPad Prism 9 (San Diego, CA, USA), with a *P* value equal or less than 0.05 considered as statistically significant (*$P \leq 0.05$, **$P \leq 0.01$,***$P \leq 0.001$, ****$P \leq 0.0001$ and ns (non-significant) when $P > 0.05$).

3. Results and discussion

Two Tz based radiolabeling precursors, Tz-PEG$_4$-HBED-CC (**4**) and Tz-PEG$_4$-DOTA (**6**), were successfully synthesized (Scheme 1). The selection of the chelators was made regarding the efficient and stable complexation with ^{68}Ga that has been indicated in various studies [2,15,17,24,25]. Although DOTA has been widely used in many applications [2,3], HBED-CC has shown faster radiolabeling kinetics with ^{68}Ga, resulting in high RCYs (>98% within 5 min) under milder reaction conditions (RT) and in higher molar activities (usually 10–37 GBq/μmol), rendering it ideal for the labeling of reactive compounds such as tetrazines, or sensitive macromolecules like proteins [41–43].

Precursor **4** was synthesized with a two-step sequence starting from Tz-PEG$_4$-NH$_2$ (**2**) and HBED-CC-tris(*tBu*)ester (**1**). The primary amine of **2** was reacted with the single free carboxylic acid group of the chelator (**1**) using the HATU coupling agent. The reaction was monitored up to two days when the highest yield was obtained. After the purification step, the intermediate (**3**) was isolated with 79% yield. The ^{1}H NMR characterization revealed the characteristic peaks of Tz at 8.57 and 7.53 ppm (Fig. S1). For the deprotection of the *tert*-butyl protecting groups, TFA was used, yielding the final product (**4**) at 98% isolated yield. The ^{1}H NMR characterization of **4** revealed disappearance of 27 protons

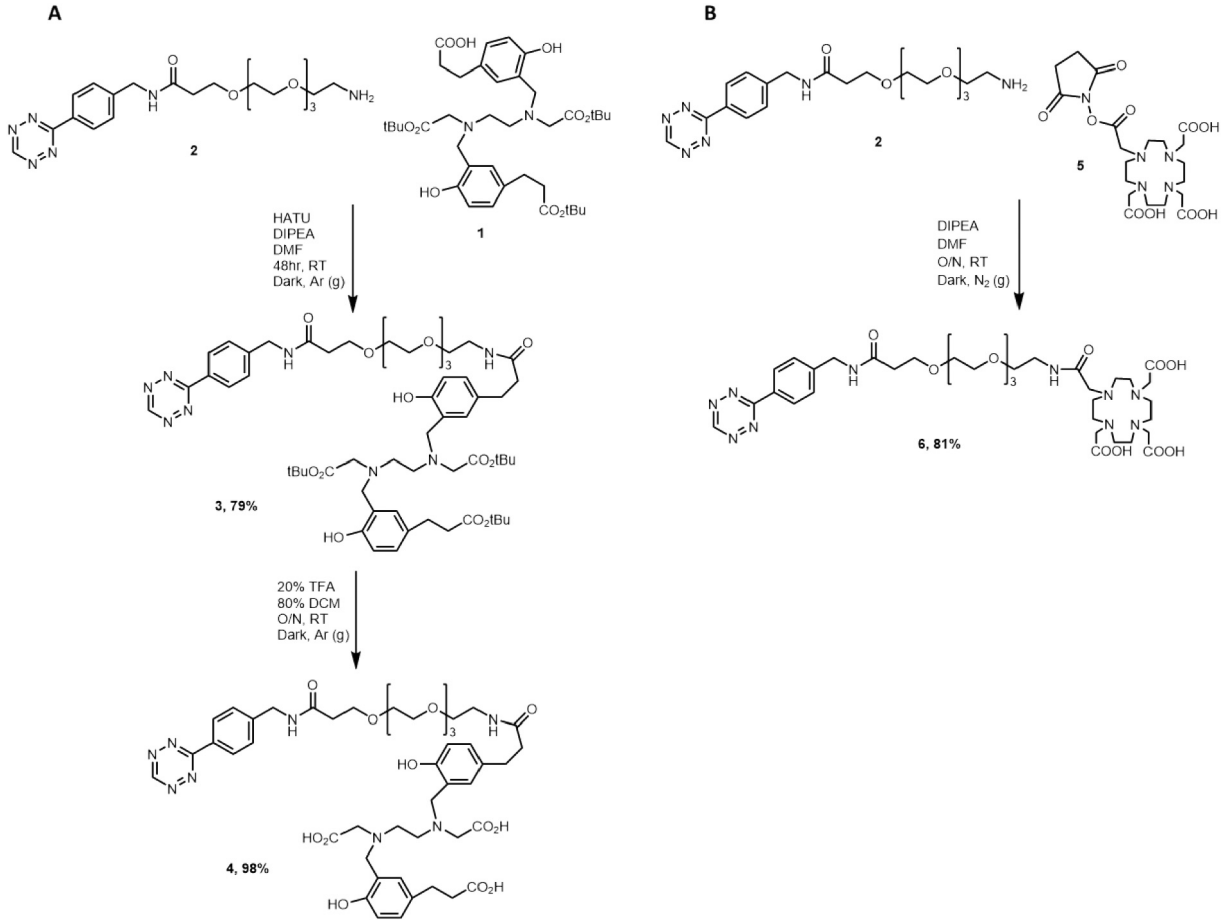

Scheme 1. Synthesis of the precursors (A) Tz-PEG$_4$-HBED-CC (**4**) and (B) Tz-PEG$_4$-DOTA (**6**). O/N: overnight and RT: room temperature.

originating from the three *tert*-butyl esters at 1.41 ppm (Fig. S3), confirming successful deprotection.

Precursor **6** was synthesized in a one-pot reaction starting from the coupling of the commercially available DOTA-NHS ester (**5**) with the primary amine of **2**, obtaining 81% yield (^{1}H NMR in Fig. S4). This was an overnight reaction and the work up and purification step of **6** were more straightforward and faster compared to **4**. The NHS ester group in the case of precursor **6** makes the coupling regioselective, and there is no need for using protected carboxylic acids and for adding a consequent extra step for the deprotection as it is required for the production of **4**.

The DOTA chelator has been a gold standard in ^{68}Ga-chemistry and has been studied extensively, including in Tz-conjugated derivatives and clinically used radiotracers [3,9,10,13]. More recently, the HBED-CC chelator has been investigated due to its higher coordination efficiency as a result of its high stability constant and acyclic nature [15,37]. It is already utilized for chelating gallium-68 in clinical production, as exemplified by [^{68}Ga]Ga-PSMA-11 (PSMA: prostate-specific membrane antigen), the first FDA approved PET radiopharmaceutical for prostate cancer imaging [44]. Therefore, in this study we were interested in comparing the synthesis and biological evaluation of Tz conjugates bearing these chelators. Various conditions were tested for the selection of the appropriate buffer and precursor amount for the ^{68}Ga-labeling of **4**. Promising results were got from the 0.1 M MES buffer (pH 4.8). The RCC was kept over 80% for almost all tested amounts of the HBED-CC precursor (**4**) as shown in Fig. 2. The amount of the precursor (**4**) for the trial reactions was varied between 10 and 700 μg, resulting in RCCs between 80 and 95%. Even higher RCCs were achieved in 2.5 M sodium acetate (pH 5.5) when using a precursor (**4**) amount between 10 and 250 μg. The resulted RCCs were over 98% even with the lowest precursor (**4**) concentration. Consequently, even lower amounts of the HBED-CC precursor (**4**) could be examined. Therefore, trials were also made using 8, 5, 1 and as low as 0.8 μg of precursor (Fig. 2). Already in the first 5 min of incubation, the RCC was >94% (97.6%, 97.6%, 96.7% and 94.3% for 8, 5, 1 and 0.8 μg, respectively), but increasing to >96% when incubated at RT up to 15 min. To achieve the maximum

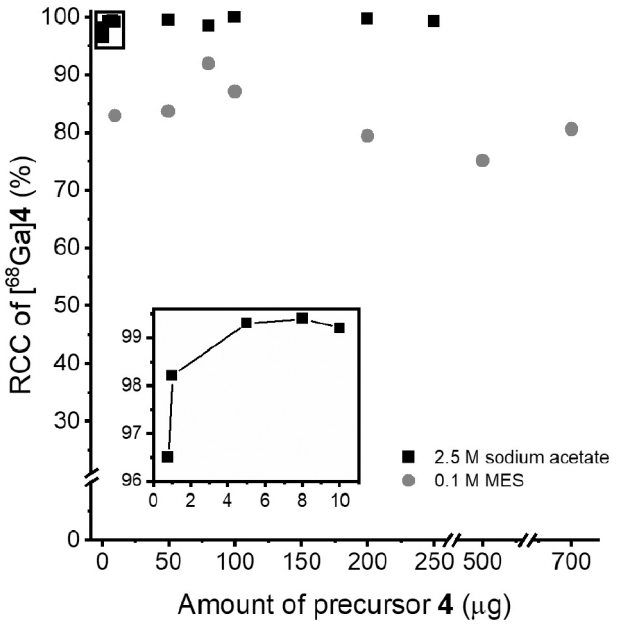

Fig. 2. The influence of the reaction buffer and precursor amount on the ^{68}Ga-radiolabeling of HBED-CC-PEG$_4$-Tz. Otherwise, the reaction conditions in all cases were the same: 0.5 ml 2.5 M sodium acetate (pH 5.5) or 0.1 M MES (pH 4.8) buffer, 60 μl ^{68}GaCl$_3$ (4.5–4.9 MBq), RT, 15 min. The RCCs were obtained from radio-TLCs. The insert represents the RCC values of the HBED-CC-PEG$_4$-Tz precursor equal to or below 10 μg in sodium acetate buffer and is denoted with a square in the main graph. The results represent the mean values (n = 1–2).

radiolabeling efficiency with RCY > 96%, 15 min of reaction time was used and a minimum 5–8 μg of precursor (**4**) was needed for a complete reaction. In the optimized conditions, 8 μg of precursor **4** was dissolved in 500 μl 2.5 M sodium acetate (pH 5.5) following the addition of the required volume of ^{68}GaCl$_3$. Depending on the experiment, the volume could be altered without influencing the RCC. In most cases, 2 ml eluate fraction containing the highest amount of radioactivity from a ^{68}Ge/^{68}Ga generator was used without further concentration. The C18 cartridge purification of the final product was done semi-automatically using a remote-controlled syringe. The RCP of the final cartridge purified product [^{68}Ga]**4** was 98.8%–99.9%.

The need to use a relatively large volume of ^{68}GaCl$_3$ solution could be overcome with concentration using an SCX (strong cation exchange) cartridge. This is an alternative method to concentrate the high volume of the eluate fraction. In this way, the whole eluted ^{68}GaCl$_3$ activity can be utilized for the reaction, and the variability in the reaction volume is negligible. ^{68}Ga is more concentrated and purer when it is added into the precursor solution. The use of the SCX cartridge enabled the setup of an automated system for the [^{68}Ga]Ga-HBED-CC-PEG$_4$-Tz ([^{68}Ga]**4**) production (supplementary material Section 1.2 and Table S1). The same reaction conditions were used as previously stated (Sections 2.6 and 2.6.1) for the manual radiosynthesis. The buffer's pH was adjusted to 4.8. The C18 cartridge purification of the final product was done semi-automatically as in the manual radiolabeling. The RCC obtained from the semi-automated synthesis of [^{68}Ga]**4** was 97.4 ± 0.7% (n = 2), matching what other research groups have reported for the ^{68}Ga-labeling of various HBED-CC precursors. Typically, the radiolabeling of HBED-CC conjugates with ^{68}Ga proceeds with an RCC of 89–98% and yields A_m = 10–37 GBq/μmol. This is the case, for instance, when antibodies and antibody fragments have been labeled [37,41,45]. Other examples of ^{68}Ga-radiolabeled HBED-CC include peptides, such as HBED-CC-c(NGR) [43,46] and HBED-CC-c(RGD) cyclic peptide conjugates [46].

The most widely known example is the radiolabeling of HBED-CC coupled with Glu-ureido-Lys, the PSMA-targeting pharmacophore, where 0.1 nmol of precursor is used for radiolabeling with ^{68}Ga, resulting in an exceptionally high RCY (>99%) and A_m (500 GBq/μmol) [47]. The radiosynthesis resulted in the very well-known [^{68}Ga]Ga-PSMA-HBED-CC prostate cancer PET tracer, currently an FDA-approved radiopharmaceutical [44]. The same group worked on the systematical comparison of [^{68}Ga]Ga-HBED-CC with [^{68}Ga]Ga-NOTA for the radiolabeling of the integrin $\alpha_v\beta_3$ peptide, RGD. Both chelators yield ^{68}Ga complexes at RT with high RCYs, but the HBED-CC labeling is more efficient and faster at low concentrations and temperatures (0.1–1.0 nmol peptide conjugates; 5 min reaction time; HBED-CC-c(RGDyK): RCY = 99%, and NOTA-c(RGDyK): RCY > 60%). Furthermore, HBED-CC has shown a higher avidity toward ^{68}Ga^{3+} at RT in direct challenge with NOTA [25]. The above observations agree with another study that compared the ^{68}Ga-labeling efficiency of recombinant proteins for PET imaging of the VEGF receptors in angiogenic vasculature using the scVEGF-PEG-HBED-CC (3 nmol, 8 min reaction time, RCY > 98%, A_m = 15 GBq/μmol) and scVEGF-PEG-NOTA (3 nmol, 8 min reaction time, RCY > 70%, A_m = 10–15 GBq/μmol) conjugates [48]. Lastly, the long-term stability of radiolabeled cyclic-NOTA (NOTA-c(RGDyK)) and acyclic-HBED-CC (HBED-CC-c(RGDyK)) chelators was examined using ^{67}Ga ($t_{½}$ = 3.26 d). The results showed a similar pattern of radiolabel stability of the two chelating agents in human serum at 37 °C. After 48 h of incubation, there was no demetallation from either of the chelates [25]. Overall, we could say that our results either concur with the ones obtained by other groups or they are of higher RCY and A_m.

In the case of the [^{68}Ga]Ga-DOTA-PEG$_4$-Tz ([^{68}Ga]**6**) tracer, precursor **6** was dissolved in 0.25 M ammonium acetate (pH 6.8) buffer. The first attempts with 100 μg and 200 μg of precursor **6**, gave a RCC of 80.4% and 97.5%, respectively. This outcome contributed to the selection of the desired amount of **6** (200 μg) for the following radiosyntheses (RCY > 88%). In a study reported by Kjaer et al., [^{68}Ga]Ga-DOTA-

PEG_{11}-Tz was produced with RCYs between 48% and 78% when using the precursor amounts between 50 and 100 μg (RCP > 90%) [3]. The results are in well accordance to our results with lower precursor amounts.

The aim of our study was to make comparison of pharmacokinetics between Tz conjugated with the two radiometal chelators. Although both precursors **4** and **6** were synthesized with high yields and leaded in straightforward radiosyntheses with high RCCs and RCYs, it is worth noticing that HBED-CC-PEG_4-Tz showed significantly faster reaction kinetics in terms of complexation with ^{68}Ga while achieving complete reactions at RT and at lower precursor concentrations, resulting also in higher molar activities. The latter would be vital for pretargeted PET imaging purposes. It would mean a lower amount of non-radiolabeled Tz molecule, thus, minimizing the consumption of TCO due to the reaction between the non-radiolabeled Tz and the TCO-functionalized macromolecule. On the other hand, for the ^{68}Ga-labeling of DOTA-PEG_4-Tz, higher precursor concentrations were necessary for attaining high RCCs and RCYs. Additionally, as it is well known, inevitably the ^{68}Ga-DOTA complex formation cannot take place at RT and for a complete reaction to occur a high temperature is required due to its macrocyclic configuration. These findings agree with the reported information on the labeling kinetics and RCYs with respect to the chelator moiety of various ^{68}Ga-labeled tracers [2,10,15,21].

After confirming the reproducibility of the high yield radiolabeling of both tracers, the *in vitro* stability was evaluated. The stability was investigated in sodium acetate buffer in the case of the HBED-CC tracer and in PBS for the DOTA tracer. The difference in the buffer selection was due to the excellent RCC of [^{68}Ga]**4** where no further purification was needed (thus, the reaction buffer was used), whereas in the case of [^{68}Ga]**6** a C18 cartridge purification was required. The stability of the radiolabel was also assessed in 20% and 50% human plasma. Furthermore, the iron challenge was performed to investigate possible transchelation between $^{68}Ga^{3+}$ and Fe^{3+} cations. In addition to their charge, the two trivalent metal cations have a very similar size. Fe^{3+} is excessively present in the blood and in the event of *in vivo* demetallation, the Fe^{3+} ion has the potential to displace ^{68}Ga in the chelator binding pocket, resulting in release of free $^{68}Ga^{3+}$ [19,20]. To investigate the competition, a high concentration of iron(III) was used (18 mM) to count as an excess for the normal iron levels in the blood (maximum physiological amount in blood for males: 32 μM [49]). [^{68}Ga]**4** gave consistent results for all the different conditions up to 5 h of incubation (Figs. 3 and S5). In all the samples, [^{68}Ga]**4** remained equal to or above 96.8% intact with only one case at 96.0% (5 h, 50% plasma). This revealed excellent *in vitro* stability for [^{68}Ga]**4**. The stability of [^{68}Ga]**6** was slightly lower; however, 90% of intact [^{68}Ga]**6** was maintained in each sample up to 5 h of incubation (Fig. 3). A single exception at 87.5% was noted for the 20% plasma sample in 5 h after the initiation of the incubation (Fig. S5). However, it should be noted that in each of the testing conditions, the [^{68}Ga]**6** was intact (equal to or above 92.7%) up to 1 h of incubation and the stability was found sufficient to proceed with the *in vivo* evaluation. [^{68}Ga]**4** $logD_{7.4}$ was -1.28 ± 0.19 ($n = 3$) and for [^{68}Ga]**6** it was slightly lower -1.45 ($n = 1$).

The *ex vivo* biodistribution of both [^{68}Ga]**4** and [^{68}Ga]**6** tracers was evaluated in BALB/c mice (Fig. 4 and supplementary material Section 2.3, Figs. S6 and S7 and Tables S2 and S3). Both tracers exhibited fast renal excretion with the highest tracer elimination between 30 and 60 min. Apart from the high activity in the gallbladder, [^{68}Ga]**4** showed increasing activity in the small intestine with a maximum %ID/g at 30 min post-injection (35.35 ± 5.07%ID/g). At the 2-hour time point (Fig. S6), an increase in accumulation was similarly observed in the large intestine (23.06 ± 2.73%ID/g). The high binding of [^{68}Ga]**4** in the intestines was the largest difference in tissue binding compared to [^{68}Ga]**6**. The denoted intestinal elimination of [^{68}Ga]**4** was due to the less hydrophilic character of the tracer ([^{68}Ga]**4** $logD_{7.4}$ was -1.28 ± 0.19 ($n = 3$) and [^{68}Ga]**6** $logD_{7.4}$ -1.45 ($n = 1$)). The structure of the HBED-CC chelator contains aromatic rings, which increase the lipophilicity of the structure directing elimination to hepatobiliary excretion. Very low accumulation of radioactivity was observed in the rest of the tissues. Thus, there was no unexpected or unusual tissue uptake. Additionally, urine samples were taken for radio-TLC measurements and there was no indication of demetallation or radiometabolites as only the intact tracer was detected. Moreover, free gallium would appear mainly in the bones, liver and lungs as well as in other undesired sites. Therefore, the *in vivo* stability of both tracers was confirmed.

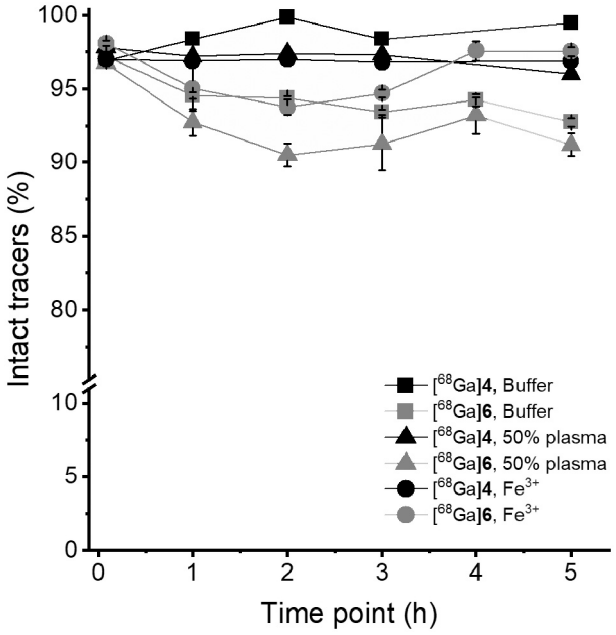

Fig. 3. *In vitro* stability of [^{68}Ga]Ga-HBED-CC-PEG_4-Tz ([^{68}Ga]**4**) and [^{68}Ga]Ga-DOTA-PEG_4-Tz ([^{68}Ga]**6**) under different conditions at 37 °C. The testing conditions were the buffer used either for the radiolabeling in the case of the HBED-CC tracer (2.5 M sodium acetate, pH 5.5) or for the formulation in the case of the DOTA tracer (10% EtOH in PBS 0.01 M, pH 7.4), 50% human plasma, and Fe^{3+} ($FeCl_3 \cdot 6H_2O$, 18 mM in MQ) for the iron challenge. The first time point was in 5 min, the next in 1 h and the reactions were monitored up to 5 h. The RCCs were obtained from radio-TLCs. The values represent the mean ± standard deviation (n = 1–3).

Furthermore, Fig. 5 demonstrates the radioactivity that was obtained in the blood at the designated time points after the injection of either [^{68}Ga]**4** or [^{68}Ga]**6**. The same trend was observed for the two tracers. A slightly higher amount of [^{68}Ga]**4** remained in the circulation compared to [^{68}Ga]**6** revealing a faster elimination of the latter which was expected due to the higher hydrophilicity. The highest radioactivity in the blood was obtained as expected in the first 15 min where the radioactivity of [^{68}Ga]**4** was 1.95 ± 0.47%ID/g and 1.36 ± 1.26%ID/g for [^{68}Ga]**6**. The major reduction in %ID/g was observed after 1 h post-injection. Both tracers were still circulating in the blood at 1 h post-injection ([^{68}Ga]**4**: 0.78 ± 0.32%ID/g and [^{68}Ga]**6**: 0.36 ± 0.20%ID/g). After 2 h of the injection, the tracer amount remaining in the blood in both cases was negligible. Overall, these findings can be translated in an appropriate timeframe regarding pretargeting. The tracers would have enough time to react *in vivo* and at the same time they would be excreted from the organism fast enough eliminating the radiation burden.

In addition, blood samples were taken from the mice after the injection of [^{68}Ga]**4** or [^{68}Ga]**6** tracer at each designated time point and the different blood components—RBCs, proteins and plasma—were separated. The percentage of radioactivity in each blood component was calculated with respect to all three components from the total activity in the sample. The results revealed a similar pattern of distribution between the blood components for the two Tz tracers (Fig. 6). The overall trend for both tracers was that the activity was gradually decreasing in

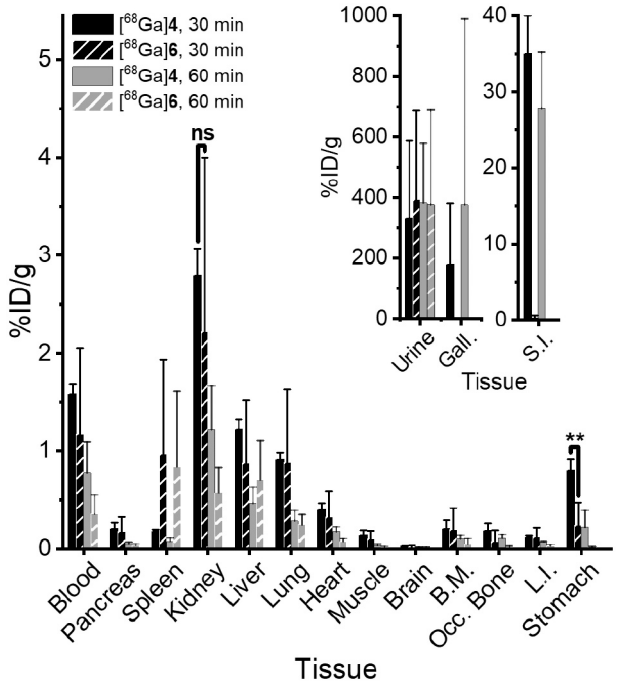

Fig. 4. Comparison of the *ex vivo* biodistribution of [^{68}Ga]Ga-HBED-CC-PEG$_4$-Tz ([^{68}Ga]**4**) and [^{68}Ga]Ga-DOTA-PEG$_4$-Tz ([^{68}Ga]**6**) at 30 and 60 min after the i.v. injection in BALB/c mice. The columns represent the mean ± standard deviation (n = 3–5). %ID/g: percent of injected dose per gram of tissue, Gall.: gallbladder, S.I.: small intestine, L.I.: large intestine, Occ. Bone: occipital bone, and B.M.: bone with marrow. Unpaired t-test was performed to assess the statistical significance of the difference in the two tracers (P = 0.0514 (ns), $^{**}P$ = 0.0049). The whole biodistribution profiles are shown in the supplementary material (Figs. S6 and S7).

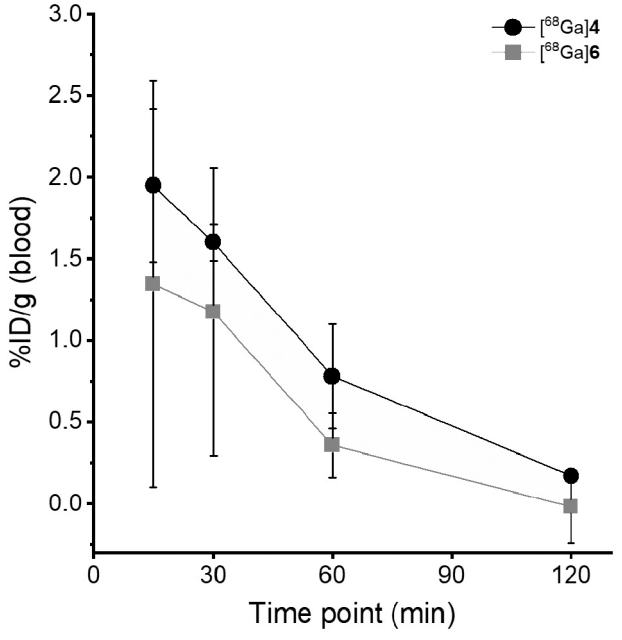

Fig. 5. Comparison of the %ID/g in blood for [^{68}Ga]Ga-HBED-CC-PEG$_4$-Tz ([^{68}Ga]**4**) and [^{68}Ga]Ga-DOTA-PEG$_4$-Tz ([^{68}Ga]**6**). The values represent the mean ± standard deviation (n = 3–5). %ID/g: percent of injected dose per gram of tissue. Unpaired t-test was performed to assess the statistical significance of the difference between two tracers (P = ns).

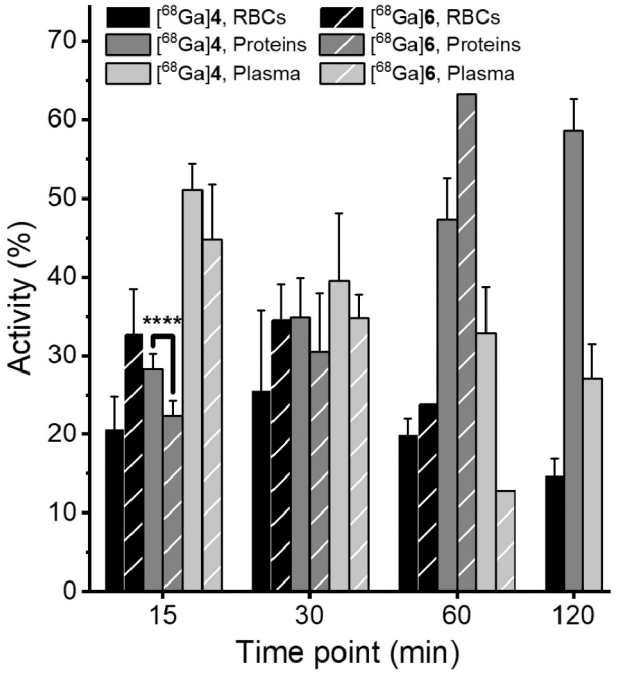

Fig. 6. The calculated activity (%) in each of the blood components after the *ex vivo* biodistribution of [^{68}Ga]Ga-HBED-CC-PEG$_4$-Tz ([^{68}Ga]**4**) (n = 3) and [^{68}Ga]Ga-DOTA-PEG$_4$-Tz ([^{68}Ga]**6**) (n = 1–5) in BALB/c mice. The results show the estimated binding of the tracer in RBCs (red blood cells), blood proteins and plasma with respect to time. The columns represent the mean ± standard deviation. Unpaired t-test was performed to assess the statistical significance of the difference in the two tracers ($^{****}P < 0.0001$).

the plasma and subsequently increasing in the blood proteins. The detected activity levels in the RBCs were comparable for each time point. Most of the obtained values were similar in all cases; around or lower than 40% was the activity obtained at all time points for both tracers in the three blood components. Exception to this observation was the activity at 15 and 60 min post-injection for both tracers in the plasma ([^{68}Ga]**4**: 51.04 ± 3.37% and [^{68}Ga]**6**: 44.78 ± 6.97%) and the blood proteins ([^{68}Ga]**4**: 47.31 ± 5.25% and [^{68}Ga]**6**: 63.25%), respectively, and at 120 min for [^{68}Ga]**4** in the proteins ([^{68}Ga]**4**: 58.36 ± 3.93%). The highest activity was found in the blood proteins due to the [^{68}Ga]**6** tracer at 60 min post injection, and this was even higher than the activity at 120 min after the [^{68}Ga]**4** injection. Overall, the activity due to the [^{68}Ga]**6** tracer was higher compared to [^{68}Ga]**4** in the RBCs and lower in both the blood proteins and the plasma with the exception at 60 min in the proteins where, however, n = 1 for [^{68}Ga]**6**. These observations agree with the blood and biodistribution profiles of the two tracers (Figs. 4 and 5, Figs. S6 and S7) which show a faster blood elimination and a lower degree of tissue binding of [^{68}Ga]**6** compared to [^{68}Ga]**4** with the exception in the spleen where the opposite was observed.

Using a short-lived radionuclide, like ^{68}Ga, to radiolabel NPs is beneficial because it provides a lower radiation burden to the subject under study (especially important in the case of long-lived macromolecules), and substantial flexibility in terms of the imaging time points. Moreover, in the case of the pretargeting concept, where the NPs are already located at the target, a short half-life radionuclide is sufficient for imaging even challenging lesions. The IEDDA reactivity of the two tracer candidates was explored using two different types of TCO-bearing nanoparticles. The nanoparticles were the porous silicon nanoparticles (PSiNPs) and Hepatitis E virus nanoparticles (HEVNPs). HEVNPs originate from the virion icosahedral HEV capsid. The NPs are RNA-independent, safe, small (<30 nm) and stable. They can be self-assembled and re-assembled, and a high accessibility for surface alterations is allowed, such as introducing an imaging agent, a targeting

ligand, or a peptide immunogen [39,50]. PSi is also a biocompatible material that can be used for the construction of engineered nanosystems. PSiNPs have a large surface area and easily adjustable pore and particle size. PSiNPs can be safely biodegraded *in vivo* into silicic acid and the rate of biodegradation can be controlled by modifications on the surface or porosity of the NPs. The surface functionalization capability differentiates PSi from other mesoporous materials. These properties make the PSiNP system suitable for applications in drug delivery and diagnosis [10,40].

The initial step was the TCO-functionalization of the NPs. The surface of the protein-based HEVNPs contains 60 lysine amino acids [39]. The primary amine of lysine can efficiently react with NHS ester, and thus, the TCO-PEG_4-NHS ester molecule was used to obtain the TCO group around the NP. Similarly, the TCO-functionalization of PSiNPs is based on the reaction between the carboxylic acid groups that are present on the PSiNPs and the TCO-PEG_3-NH_2 reagent. Different conditions were investigated to find the optimal amounts and molar ratios of the NPs and the TCO reagents.

Consequently, the *in vitro* Tz-TCO ligation reaction was explored in both NP cases. When the [^{68}Ga]Ga-DOTA-PEG_4-Tz ([^{68}Ga]**6**) was used, the IEDDA RCCs were only 7.7–9.6%. The low IEDDA RCC could be a consequence of the lower molar activity of [^{68}Ga]**6** compared with [^{68}Ga]**4**. A higher amount of the precursor **6** is needed for achieving high ^{68}Ga-labeling yields, leading to a lower molar activity. In the IEDDA reaction, this would result in a higher amount of non-radiolabeled Tz that would be available to block the TCO binding sites while reacting with them in place of the radiolabeled Tz, thus, greatly influencing the IEDDA reaction efficiency. Moreover, the most common TCO:Tz ratio in pretargeting (1:1) in the case of TCO-conjugated antibodies, is not always ideal for TCO-conjugated NPs [53]. Therefore, in our study, different TCO:Tz ratios were used to examine the *in vitro* IEDDA ligation aiming at the highest TCO:Tz ratio possible. Because of the low IEDDA RCCs resulting from [^{68}Ga]**6**, most of the radiolabeling of the NPs was done with [^{68}Ga]Ga-HBED-CC-PEG_4-Tz ([^{68}Ga]**4**). For this reason, the discussion from this point will be based on the [^{68}Ga]**4**-labeled NPs. The IEDDA reaction kinetics for [^{68}Ga]**4** was monitored by radio-TLC from 10 min and up to 1 h (examples of chromatograms: supplementary material Section 2.4, Fig. S8). However, because no difference was noticed in the RCC at longer incubations, the 10 min reaction time was chosen. Fig. 7 illustrates the main findings regarding the influence of [^{68}Ga]Ga-HBED-CC-PEG_4-Tz amount on IEDDA while keeping the same amount of NPs. From the graph (Fig. 7), the TCO moles could be estimated with respect to the Tz moles when the amount of the Tz used gave a plateau of the lowest RCC values. Thus, the TCO moles were at least 100 nmol per mg of PSiNPs (for min. 10.3 nmol of Tz) and minimum 55 nmol per mg of HEVNPs (for min. 2.2 nmol of Tz). For both NPs, a higher RCC was achieved with a decreasing amount of the Tz tracer (higher TCO:Tz ratio), and thus, a higher molar activity. Additionally, for higher than 1 nmol of Tz, the [^{68}Ga]**4**-TCO-HEVNPs RCCs were lower than 5% following the 10 min reaction time. The majority of the highest [^{68}Ga]**4**-TCO-HEVNPs RCCs (around 20%) were very closely associated to the lowest RCC of [^{68}Ga]**4**-TCO-PSiNPs. Moreover, the highest RCC for the [^{68}Ga]**4**-TCO-PSiNPs was confirmed to be around 60% in multiple trials. More consistent results were obtained from the *in vitro* reaction between the TCO-PSiNPs and [^{68}Ga]**4** compared to the TCO-HEVNPs and [^{68}Ga]**4** case. Despite the fact that the conjugation between the TCO molecule and HEVNPs was attempted using numerous different reaction conditions by altering the buffer (phosphate buffers, borate, sodium carbonate) and the purification techniques (dialysis membranes, HPLC (with a size exclusion chromatography column) and desalting columns with either glucan (Sephadex) or polypropylene resin), there was no improvement in the reaction efficiency as it was noticed from the obtained RCCs following the consequent IEDDA trials. Therefore, because the conjugation was more effective for PSiNPs, they were further tested in tumor-mimicking conditions for illustrating the potential of [^{68}Ga]**4** for pretargeted imaging applications. The TCO-

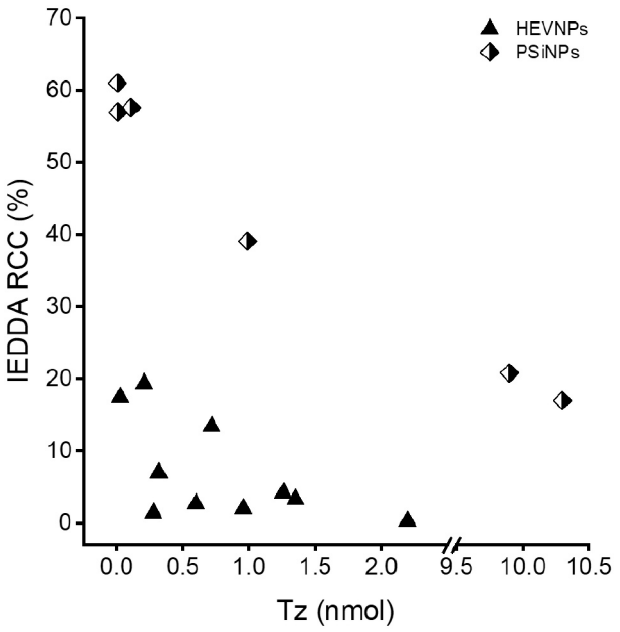

Fig. 7. The influence of the tetrazine [^{68}Ga]**4** amount on the RCC obtained from the *in vitro* IEDDA while keeping the amount of NPs, and thus TCO, constant (10 min reaction time). The illustration shows the outcome from the reaction using both NP types, HEVNPs and PSiNPs. The data represents single values. IEDDA RCC represents the RCC obtained after inverse electron demand Diels-Alder reactions between the Tz tracer ([^{68}Ga]Ga-HBED-CC-PEG_4-Tz) and the functionalized NPs (TCO-HEVNPs or TCO-PSiNPs).

PSiNPs were incubated up to 24 h in either sodium acetate pH 5.3, or 10% FBS in sodium acetate pH 5.3. Both buffers mimic the human tumor microenvironment. The acetate buffer (pH 5.2 ± 1) has been used to mimic the acidic late endosome intracellularly [54], and FBS has routinely been utilized for culturing various cell types due to its known effects on cell growth [55]. Following the incubation of the NPs in the tumor-simulating fluids at different time points, TCO-PSiNPs were reacted with [^{68}Ga]Ga-HBED-CC-PEG_4-Tz. The outcome (supplementary material Section 2.5, Fig. S9) showed that IEDDA was still feasible even after treating the NPs in tumor-mimicking conditions, and thus, it can be concluded that [^{68}Ga]**4** looks promising regarding the *in vivo* preclinical imaging applications. Stéen et al. recently reported, that the reduced lipophilicity of a Tz-tracer and high IEDDA reactivity are the key parameters for the *in vivo* performance of tetrazines in pretargeted PET imaging [51,52]. The observation was based on their investigation on several tetrazine derivatives in pretargeted PET imaging of LS174T tumor xenografts after injection of CC49-TCO. The measured tumor-to-muscle ratios were significantly lower for tetrazines with $clogD_{7.4} > 0$. The highest ratios were reported for tetrazines with $clogD_{7.4}$ between −0.99 and (−1.53). The measured $logD_{7.4}$ of [^{68}Ga]**4** = −1.28 ± 0.19 is between this range further warranting future evaluation of [^{68}Ga]**4** as a tracer for pretargeted PET imaging.

4. Conclusions

In conclusion, two ^{68}Ga-radiolabeled tetrazine tracers were synthesized and their biodistribution was evaluated in mice. Excellent RCCs and RCYs were obtained especially for [^{68}Ga]Ga-HBED-CC-PEG_4-Tz. High radiolabel stability of [^{68}Ga]**4** or [^{68}Ga]**6** at physiological conditions was reported. The *ex vivo* biodistribution of [^{68}Ga]**4** and [^{68}Ga]**6** revealed fast renal excretion. Additionally, in the case of [^{68}Ga]**4** increased radioactivity was detected in the intestine due to the more hydrophobic character of this tracer ($logD_{7.4}$ of [^{68}Ga]**4** = −1.28 ± 0.19). Lastly, the *in vitro* IEDDA reaction between the two tetrazine tracers and two different types of NPs was assessed. Using a short-lived

radionuclide like ^{68}Ga to radiolabel NPs is beneficial because it offers a lower radiation burden to the organism, and substantial flexibility in terms of the imaging time points. The *in vitro* IEDDA reactivity was confirmed although optimization of the reaction conditions is still needed. Overall, [^{68}Ga]Ga-HBED-CC-PEG$_4$-Tz was shown to be superior compared to [^{68}Ga]Ga-DOTA-PEG$_4$-Tz in terms of radiolabeling efficiency and molar activity, increasing the sensitivity of the tracer to detect a targeting vector even with a low TCO concentration.

Abbreviations

Tz	tetrazine
HBED-CC	*N,N′*-bis-[2-hydroxy-5-(carboxyethyl)benzyl] ethylenediamine-N,N′-diacetic acid
DOTA	1,4,7,10-tetraazacyclododecane-1,4,7,10-tetraacetic acid
IEDDA	inverse electron demand Diels-Alder
TCO	*trans*-cyclooctene
HEVNPs	hepatitis E virus nanoparticles
PSiNPs	porous silicon nanoparticles
HATU	1-[bis(dimethylamino)methylene]-1H-1,2,3-triazolo[4,5-*b*] pyridinium 3-oxid hexafluorophosphate
DIPEA	N,N-diisopropylethylamine
FA	formic acid
RT	room temperature
O/N	overnight
iTLC-SA	instant thin layer chromatography-silicic acid
%ID/g	percent of injected dose per gram (tissue)
Gall.	gallbladder
S.I.	small intestine
L.I.	large intestine.
Occ. Bone	occipital bone
B.M.	bone with marrow
ns	non-significant
RBCs	red blood cells

Acknowledgements

This work was financially supported by the Academy of Finland (decision numbers: 298481, 278056, 318422, and 320102), US National Institutes of Health (TR002866, CA198880, CA225266, EB021230), National Institute of Food and Agriculture (CADMCB-7399-H), FiPro and UC STAIR programs. The authors would like to thank Prof. Jarno Salonen and Ermei Mäkilä for providing PSiNPs for the *in vitro* evaluation of IEDDA. Dr. C.-C. Cheng and Mo Baikoghli are acknowledged for the HEVNPs synthesis and characterization. The authors would also like to thank Kirsi Kepsu and Dr. Teija Koivula for their support and technical advice on the automated system for the synthesis of the [^{68}Ga]Ga-HBED-CC-PEG$_4$-Tz tracer.

Appendix A. Supplementary data

Supplementary data to this article can be found online at https://doi.org/10.1016/j.nucmedbio.2022.05.004.

References

[1] Velikyan I. Prospective of 68Ga-radiopharmaceutical development. Theranostics 2013;4:47–80. https://doi.org/10.7150/thno.7447.
[2] Kilian K. 68Ga-DOTA and analogs: current status and future perspectives. Rep Pract Oncol Radiother 2014;19:S13–21. https://doi.org/10.1016/j.rpor.2014.04.016.
[3] Edem PE, Jørgensen JT, Nørregaard K, Rossin R, Yazdani A, Valliant JF, et al. Evaluation of a 68Ga-labeled DOTA-tetrazine as a PET alternative to 111In-SPECT pretargeted imaging. Mol Basel Switz 2020;25. https://doi.org/10.3390/molecules25030463.
[4] Altai M, Membreno R, Cook B, Tolmachev V, Zeglis BM. Pretargeted imaging and therapy. J Nucl Med 2017;58:1553–9. https://doi.org/10.2967/jnumed.117.189944.
[5] Hou S, Choi J, Garcia MA, Xing Y, Chen K-J, Chen Y-M, et al. Pretargeted positron emission tomography imaging that employs supramolecular nanoparticles with in vivo bioorthogonal chemistry. ACS Nano 2016;10:1417–24. https://doi.org/10.1021/acsnano.5b06860.
[6] Summer D, Mayr S, Petrik M, Rangger C, Schoeler K, Vieider L, et al. Pretargeted imaging with Gallium-68—improving the binding capability by increasing the number of tetrazine motifs. Pharmaceuticals 2018;11. https://doi.org/10.3390/ph11040102.
[7] Oliveira BL, Guo Z, Bernardes GJL. Inverse electron demand Diels-Alder reactions in chemical biology. Chem Soc Rev 2017;46:4895–950. https://doi.org/10.1039/C7CS00184C.
[8] Zeglis BM, Sevak KK, Reiner T, Mohindra P, Carlin SD, Zanzonico P, et al. A pretargeted PET imaging strategy based on bioorthogonal diels-Alder click chemistry. J Nucl Med Off Publ Soc Nucl Med 2013;54:1389–96. https://doi.org/10.2967/jnumed.112.115840.
[9] Evans HL, Nguyen Q-D, Carroll LS, Kaliszczak M, Twyman FJ, Spivey AC, et al. A bioorthogonal 68Ga-labelling strategy for rapid in vivo imaging. Chem Commun 2014;50:9557–60. https://doi.org/10.1039/C4CC03903C.
[10] Lumen D, Näkki S, Imlimthan S, Lambidis E, Sarparanta M, Xu W, et al. Site-specific 111In-radiolabeling of dual-PEGylated porous silicon nanoparticles and their in vivo evaluation in murine 4T1 breast cancer model. Pharmaceutics 2019;11. https://doi.org/10.3390/pharmaceutics11120686.
[11] Otaru S, Imlimthan S, Sarparanta M, Helariutta K, Wähälä K, Airaksinen AJ. Evaluation of organo [18F]fluorosilicon tetrazine as a prosthetic group for the synthesis of PET radiotracers. Molecules 2020;25:1208. https://doi.org/10.3390/molecules25051208.
[12] Keinänen O, Fung K, Brennan JM, Zia N, Harris M, van Dam E, et al. Harnessing 64Cu/67Cu for a theranostic approach to pretargeted radioimmunotherapy. Proc Natl Acad Sci 2020;117:28316–27. https://doi.org/10.1073/pnas.2009960117.
[13] Rossin R, Renart Verkerk P, van den Bosch SM, Vulders RCM, Verel I, Lub J, et al. In vivo chemistry for pretargeted tumor imaging in live mice. Angew Chem Int Ed 2010;49:3375–8. https://doi.org/10.1002/anie.200906294.
[14] Stéen EJL, Edem PE, Nørregaard K, Jørgensen JT, Shalgunov V, Kjaer A, et al. Pretargeting in nuclear imaging and radionuclide therapy: improving efficacy of theranostics and nanomedicines. Biomaterials 2018;179:209–45. https://doi.org/10.1016/j.biomaterials.2018.06.021.
[15] Spang P, Herrmann C, Roesch F. Bifunctional Gallium-68 chelators: past, present, and future. Semin Nucl Med 2016;46:373–94. https://doi.org/10.1053/j.semnuclmed.2016.04.003.
[16] Breeman WAP, de Blois E, Sze Chan H, Konijnenberg M, Kwekkeboom DJ, Krenning EP. 68Ga-labeled DOTA-peptides and 68Ga-labeled radiopharmaceuticals for positron emission tomography: current status of research, clinical applications, and future perspectives. Semin Nucl Med 2011;41:314–21. https://doi.org/10.1053/j.semnuclmed.2011.02.001.
[17] Berry DJ, Ma Y, Ballinger JR, Tavaré R, Koers A, Sunassee K, et al. Efficient bifunctional gallium-68 chelators for positron emission tomography: tris (hydroxypyridinone) ligands. Chem Commun Camb Engl 2011;47:7068–70. https://doi.org/10.1039/c1cc12123e.
[18] Autio A, Virtanen H, Tolvanen T, Liljenbäck H, Oikonen V, Saanijoki T, et al. Absorption, distribution and excretion of intravenously injected (68)Ge/(68)Ga generator eluate in healthy rats, and estimation of human radiation dosimetry. EJNMMI Res 2015;5:117. https://doi.org/10.1186/s13550-015-0117-z.
[19] Mjos KD, Cawthray JF, Polishchuk E, Abrams MJ, Orvig C. Gallium(III) and iron (III) complexes of quinolone antimicrobials. Dalton Trans 2016;45:13146–60. https://doi.org/10.1039/C6DT01315E.
[20] Silvola JM, Laitinen I, Sipilä HJ, Laine VJO, Leppänen P, Ylä-Herttuala S, et al. Uptake of 68gallium in atherosclerotic plaques in LDLR-/-ApoB100/100 mice. EJNMMI Res 2011;1:14. https://doi.org/10.1186/2191-219X-1-14.
[21] Banerjee SR, Pomper MG. Clinical applications of Gallium-68. Appl Radiat Isot Data Instrum Methods Use Agric Ind Med 2013:2–13. https://doi.org/10.1016/j.apradiso.2013.01.039.
[22] Meyer J-P, Tully KM, Jackson J, Dilling TR, Reiner T, Lewis JS. Bioorthogonal masking of circulating antibody-TCO groups using tetrazine-functionalized dextran polymers. Bioconjug Chem 2018;29:538–45. https://doi.org/10.1021/acs.bioconjchem.8b00028.
[23] Litau S, Seibold U, Wängler B, Schirrmacher R, Wängler C. iEDDA conjugation reaction in radiometal labeling of peptides with 68Ga and 64Cu: unexpected findings. ACS Omega 2018;3:14039–53. https://doi.org/10.1021/acsomega.8b01926.
[24] Prince D, Rossouw D, Rubow S. Optimization of a labeling and kit preparation method for Ga-68 labeled DOTATATE, using cation exchange resin purified Ga-68 eluates obtained from a tin dioxide 68Ge/68Ga generator. Mol Imaging Biol 2018;20:1008–14. https://doi.org/10.1007/s11307-018-1195-x.
[25] Eder M, Neels O, Müller M, Bauder-Wüst U, Remde Y, Schäfer M, et al. Novel preclinical and radiopharmaceutical aspects of [68Ga]Ga-PSMA-HBED-CC: a new PET tracer for imaging of prostate cancer. Pharm Basel Switz 2014;7:779–96. https://doi.org/10.3390/ph7070779.
[26] Makarem A, Konrad M, Liolios C, Kopka K. A convenient synthesis for HBED-CC-tris(tert-butyl ester). Synlett 2018;29:1239–43. https://doi.org/10.1055/s-0036-1591950.
[27] Makarem A, Sarvestani MK, Klika KD, Kopka K. A multifunctional HBED-type chelator with dual conjugation capabilities for radiopharmaceutical development. Synlett 2019;30:1795–8. https://doi.org/10.1055/s-0039-1690194.
[28] Zha Z, Wu Z, Choi SR, Ploessl K, Smith M, Alexoff D, et al. A new [68Ga]Ga-HBED-CC-bisphosphonate as a bone imaging agent. Mol Pharm 2020;17:1674–84. https://doi.org/10.1021/acs.molpharmaceut.0c00103.
[29] Trencsényi G, Dénes N, Nagy G, Kis A, Vida A, Farkas F, et al. Comparative preclinical evaluation of 68Ga-NODAGA and 68Ga-HBED-CC conjugated

procainamide in melanoma imaging. J Pharm Biomed Anal 2017;139:54–64. https://doi.org/10.1016/j.jpba.2017.02.049.
[30] Hong H, Ploessl K, Zha Z, Wang H, Guo R, Xie Q, et al. Development and validation of a kit formulation of [68Ga]Ga-P15-041 as a bone imaging agent. Appl Radiat Isot 2021;169:109485. https://doi.org/10.1016/j.apradiso.2020.109485.
[31] Liolios C, Buchmuller B, Bauder-Wüst U, Schäfer M, Leotta K, Haberkorn U, et al. Monomeric and dimeric 68Ga-labeled bombesin analogues for positron emission tomography (PET) imaging of tumors expressing gastrin-releasing peptide receptors (GRPrs). J Med Chem 2018;61:2062–74. https://doi.org/10.1021/acs.jmedchem.7b01856.
[32] Klika KD, Pieve CD, Kopka K, Smith G, Makarem A. Synthesis and application of a thiol-reactive HBED-type chelator for development of easy-to-produce Ga-radiopharmaceutical kits and imaging probes. Org Biomol Chem 2021;19:1722–6. https://doi.org/10.1039/D0OB02513E.
[33] Choi PS, Lee JY, Park JH, Kim SW. Synthesis and evaluation of 68Ga-HBED-CC-EDBE-folate for positron-emission tomography imaging of overexpressed folate receptors on CT26 tumor cells. J Label Compd Radiopharm 2018;61:4–10. https://doi.org/10.1002/jlcr.3563.
[34] Jerzyk K, Kludkiewicz D, Pijarowska-Kruszyna J, Jaron A, Maurin M, Sikora A, et al. Synthesis of HBED–CC–tris(tert-butyl ester) using a solid phase and a microwave reactor. Tetrahedron 2021;84:132018. https://doi.org/10.1016/j.tet.2021.132018.
[35] S Shi L Yao L Li Z Wu Z Zha HF Kung et al Synthesis of novel technetium-99m tricarbonyl-HBED-CC complexes and structural prediction in solution by density functional theory calculation. R Soc Open Sci n.d.;6:191247. doi:10.1098/rsos.191247.
[36] Pyka T, Weirich G, Einspieler I, Maurer T, Theisen J, Hatzichristodoulou G, et al. 68Ga-PSMA-HBED-CC PET for differential diagnosis of suggestive lung lesions in patients with prostate cancer. J Nucl Med Off Publ Soc Nucl Med 2016;57:367–71. https://doi.org/10.2967/jnumed.115.164442.
[37] Eder M, Wängler B, Knackmuss S, LeGall F, Little M, Haberkorn U, et al. Tetrafluorophenolate of HBED-CC: a versatile conjugation agent for 68Ga-labeled small recombinant antibodies. Eur J Nucl Med Mol Imaging 2008;35:1878–86. https://doi.org/10.1007/s00259-008-0816-z.
[38] Sathekge M, Lengana T, Modiselle M, Vorster M, Zeevaart J, Maes A, et al. 68Ga-PSMA-HBED-CC PET imaging in breast carcinoma patients. Eur J Nucl Med Mol Imaging 2017;44:689–94. https://doi.org/10.1007/s00259-016-3563-6.
[39] Chen C-C, Xing L, Stark M, Ou T, Holla P, Xiao K, et al. Chemically activatable viral capsid functionalized for cancer targeting. Nanomed 2016;11:377–90. https://doi.org/10.2217/nnm.15.207.
[40] Lumen D, Wang S, Mäkilä E, Imlimthan S, Sarparanta M, Correia AMR, et al. Investigation of silicon nanoparticles produced by centrifuge chemical vapor deposition for applications in therapy and diagnostics. Eur J Pharm Biopharm 2021;158:254–65. https://doi.org/10.1016/j.ejpb.2020.11.022.
[41] Shi S, Zhang L, Wu Z, Zhang A, Hong H, Choi SR, et al. [68Ga]Ga-HBED-CC-DiAsp: a new renal function imaging agent. Nucl Med Biol 2020;82–83:17–24. https://doi.org/10.1016/j.nucmedbio.2019.12.005.
[42] Liolios C, Shegani A, Roupa I, Kiritsis C, Makarem A, Paravatou-Petsotas M, et al. Synthesis, characterization and evaluation of 68Ga labelled monomeric and dimeric quinazoline derivatives of the HBED-CC chelator targeting the epidermal growth factor receptor. Bioorganic Chem 2020;100:103855. https://doi.org/10.1016/j.bioorg.2020.103855.
[43] Satpati D, Sharma R, Sarma HD, Dash A. Comparative evaluation of 68Ga-labeled NODAGA, DOTAGA, and HBED-CC-conjugated cNGR peptide chelates as tumor-targeted molecular imaging probes. Chem Biol Drug Des 2018;91:781–8. https://doi.org/10.1111/cbdd.13143.
[44] Fendler WP, Calais J, Eiber M, Flavell RR, Mishoe A, Feng FY, et al. Assessment of 68Ga-PSMA-11 PET accuracy in localizing recurrent prostate cancer: a prospective single-arm clinical trial. JAMA Oncol 2019;5:856–63. https://doi.org/10.1001/jamaoncol.2019.0096.
[45] Eder M, Knackmuss S, Le Gall F, Reusch U, Rybin V, Little M, et al. 68Ga-labelled recombinant antibody variants for immuno-PET imaging of solid tumours. Eur J Nucl Med Mol Imaging 2010;37:1397–407. https://doi.org/10.1007/s00259-010-1392-6.
[46] Satpati D, Sharma R, Kumar C, Dev Sarma H, Dash A. 68 ga-chelation and comparative evaluation of N, N ′-bis-[2-hydroxy-5-(carboxyethyl)benzyl] ethylenediamine- N, N ′-diacetic acid (HBED-CC) conjugated NGR and RGD peptides as tumor targeted molecular imaging probes. MedChemComm 2017;8:673–9. https://doi.org/10.1039/C7MD00006E.
[47] Schäfer M, Bauder-Wüst U, Leotta K, Zoller F, Mier W, Haberkorn U, et al. A dimerized urea-based inhibitor of the prostate-specific membrane antigen for 68Ga-PET imaging of prostate cancer. EJNMMI Res 2012;2:23. https://doi.org/10.1186/2191-219X-2-23.
[48] Eder M, Krivoshein AV, Backer M, Backer JM, Haberkorn U, Eisenhut M. ScVEGF-PEG-HBED-CC and scVEGF-PEG-NOTA conjugates: comparison of easy-to-label recombinant proteins for [68Ga]PET imaging of VEGF receptors in angiogenic vasculature. Nucl Med Biol 2010;37:405–12. https://doi.org/10.1016/j.nucmedbio.2010.02.001.
[49] Pagana KD, Pagana TJ, Pagana TN. Mosby's diagnostic and laboratory test reference. 2015.
[50] Cheng RH. Hepatitis E nanoparticle: a capsid-based platform for non-invasive vaccine delivery and imaging-guided cancer treatment. Adv Res Gastroenterol Hepatol 2018;9. https://doi.org/10.19080/ARGH.2018.09.555752.
[51] Stéen EJL, Jørgensen JT, Denk C, Battisti UM, Nørregaard K, Edem PE, et al. Lipophilicity and click reactivity determine the performance of bioorthogonal tetrazine tools in pretargeted in vivo chemistry. ACS Pharmacol Transl Sci 2021;4:824–33. https://doi.org/10.1021/acsptsci.1c00007.
[52] Stéen EJL, Jørgensen JT, Johann K, Nørregaard K, Sohr B, Svatunek D, et al. Trans-cyclooctene-functionalized PeptoBrushes with improved reaction kinetics of the tetrazine ligation for pretargeted nuclear imaging. ACS Nano 2020;14:568–84. https://doi.org/10.1021/acsnano.9b06905.
[53] Keinänen O, Mäkilä EM, Lindgren R, Virtanen H, Liljenbäck H, Oikonen V, et al. Pretargeted PET imaging of trans-cyclooctene-modified porous silicon nanoparticles. ACS Omega 2017;2:62–9. https://doi.org/10.1021/acsomega.6b00269.
[54] Emamzadeh M, Pasparakis G. Polymer coated gold nanoshells for combinational photochemotherapy of pancreatic cancer with gemcitabine. Sci Rep 2021;11:9404. https://doi.org/10.1038/s41598-021-88909-x.
[55] Villasante A, Robinson ST, Cohen AR, Lock R, Guo XE, Vunjak-Novakovic G. Human serum enhances biomimicry of engineered tissue models of bone and cancer. Front Bioeng Biotechnol 2021;9:506. https://doi.org/10.3389/fbioe.2021.658472.